Soft Matter

RSC Publishing

PAPER

View Article Online
View Journal | View Issue

Electric field driven self-assembly of ionic microgels

Cite this: *Soft Matter*, 2013, **9**, 9199

Sofi Nöjd,[a] Priti S. Mohanty,*[a] Payam Bagheri,[b] Anand Yethiraj[b] and Peter Schurtenberger[a]

We study, using fluorescent confocal laser scanning microscopy, the directed self-assembly of cross-linked ionic microgels under the influence of an applied alternating electric field at different effective packing fractions ϕ_{eff} in real space. We present a detailed description of the contribution of the electric field to the soft interparticle potential, and its influence on the phase diagram as a function of ϕ_{eff} and field strength E at a constant frequency of 100 kHz. In our previous work [Mohanty *et al.*, *Soft Matter*, 2012, **8**, 10819], we demonstrated the existence of field-induced structural transitions both at low and high ϕ_{eff}. In this work, we revisit the phase behavior at low and intermediate ϕ_{eff} with a focus on both structure and dynamics. We demonstrate the existence of various field induced transitions such as an isotropic fluid to string phase to body centered tetragonal (BCT) crystal phase at low concentrations and a reversible field-induced crystal (face centered cubic, FCC) to crystal (BCT) transition at intermediate concentrations. We also investigate the kinetics of the crystal–crystal transition and demonstrate that this occurs through an intermediate melting process. These results are discussed in the light of previous studies of dipolar hard and charged colloids.

Received 2nd May 2013
Accepted 3rd July 2013

DOI: 10.1039/c3sm51226f

www.rsc.org/softmatter

1 Introduction

Directed self-assembly of colloids using external electric fields is a promising route towards the development of three-dimensional (3D) ordered structures with different symmetries,[1–7] with potential applications in advanced materials such as electrorheological fluids or photonic crystals. When an external electric field is applied to a colloidal suspension, the particles acquire an electric dipole moment as a result of the mismatch of the permittivity of the particle with that of the solvent and, as a result, they form elongated structures that align along the field direction. This field-induced string formation has dramatic consequences for the rheological properties, and these suspensions are thus called electrorheological (ER) fluids.[8,9] The electric field-induced phase behavior in colloidal suspensions is mostly governed by an interplay between hard-sphere repulsions and the dipole–dipole interaction, whose strength can be tuned by the magnitude of the electric field.[1–5,9–15] The addition of electrostatic repulsions in addition to the hard-sphere and dipolar interaction has been shown to produce even more complex crystal phases along with the possibility of crystal-to-crystal transitions.[4,13]

"Soft" colloids,[16–18] where the center to center distance a_s can be smaller than the diameter σ_o, are an interesting alternative to the previously studied hard-sphere-like and charged colloids. The intrinsic softness of the particles gives rise to a finite repulsion at or beyond contact, and such soft colloids have recently attracted considerable interest within the experimental and theoretical soft matter community. In particular, cross-linked microgels such as poly(*N*-isopropylacrylamide) (PNIPAM) have frequently been used as an excellent model system for soft colloids.[19–26] As a result of the soft potential, microgels can be packed to an effective volume fraction ϕ_{eff} far above closed packing $\phi_{cp} \approx 0.74$ expected for non-deformable hard spheres, with enormous consequences for the resulting structural and dynamic properties.

Ionic microgels are yet another interesting class of soft colloids, where the effective interaction potential crosses over from a Yukawa type interaction at large inter-particle distances $a_s \gg \sigma_o$ to a much softer one at short distances $a_s \lesssim \sigma_o$.[27–29] This soft-repulsive interaction is expected to dominate at high ϕ_{eff}, and theory has shown that a very rich phase behavior exists with many new crystalline phases appearing.[28] In a previous study,[30] we have demonstrated that ionic microgels can be used as a promising model system to study dipolar interactions in suspensions of soft particles. We in particular observed field-induced structural transitions from a glassy state to crystal and to an arrested phase separated state at $\phi_{eff} > \phi_{cp}$. In the case of charged hard-core spherical particles such as polystyrene colloids in aqueous suspensions under an external AC field, the dipolar interaction at lower frequencies (~kHz range) is a sum of the contributions from ionic polarization arising from the surface charges in the double layer and dielectric polarization

[a]*Physical Chemistry, Department of Chemistry, Lund University, Lund, Sweden. E-mail: priti.mohanty@fkem1.lu.se*

[b]*Department of Physics and Physical Oceanography, Memorial University, St. John's, NL, Canada*

arising from differences in the dielectric constant between particles and solvent.[7,31] At high frequencies (~MHz range), primarily studied with charged hard-core colloidal spheres in both aqueous and low polar solvents, the contribution from ionic polarization is reduced and the field-induced interaction is thought to be governed primarily by dielectric polarization.[3–6]

In contrast to these traditional colloidal systems, ionic microgels in the swollen state contain more than 80% of water, and the dielectric permittivity difference between the particle and water is likely too small to result in a significant dielectric polarization in the presence of an external electric field. Given the fact that ionic microgels contain significantly higher amounts of confined counterions compared to the number of surface charges,[29] we believe that the dominant contribution comes from the polarization of confined counterions.

So far, the phase behavior at intermediate $\phi_{\mathrm{eff}} \lesssim \phi_{\mathrm{cp}}$ has remained unexplored. Hence this motivated us to carry out field studies at intermediate concentrations. In the present work, we use ionic microgels of PNIPAM-*co*-PAA. The particles have a low polydispersity when compared to the microgels used in our previous study, and they have a larger cross-linking density of 5 mol%. Here, we explore the structure formation and dynamics at $0.07 \leq \phi_{\mathrm{eff}} \leq 0.66$ under the influence of a uniaxial alternating electric field at a constant frequency of 100 kHz using confocal microscopy.

2 Materials and methods

2.1 Synthesis and particle characterization

We use fluorescently labeled PNIPAM based ionic microgels as a model system to study the electric field driven self-assembly at different packing fractions using confocal laser scanning microscopy (CLSM). Ionic microgel particles were synthesized by free-radical precipitation polymerization[30] using *N*-isopropylacrylamide (NIPAM) as the monomer, *N*,*N*-methylene-bis-acrylamide as a cross-linker, and methacryloxyethyl thiocarbamoyl rhodamine B (MRB) as a covalently linked fluorescent label. Acrylic acid was used as an ionic co-monomer. The cross-linking density of the particles was 5 mol%, and the polydispersity was 5%. The samples were fully de-ionized using ion exchange resins.

Dynamic and static light scattering studies were carried out in the swollen state at a temperature of 20 °C using a modulated 3D cross-correlation DLS instrument (LS Instruments, Switzerland). The hydrodynamic radius ($R_{\mathrm{DLS}} = 530$ nm) was extracted using a first order cumulant analysis[26] from the measured intensity cross-correlation function. The particle form factor measured by static light scattering (SLS) was fitted with the so-called fuzzy sphere model.[20] From the fit we obtained a core radius of $R_{\mathrm{core}} = 337$ nm, a fuzzy shell thickness of $2\sigma_{\mathrm{surf}} = 20$ nm and thus an overall radius of $R_{\mathrm{SLS}} = 357$ nm. A comparison of the size of the ionic microgel in the swollen state (at $T = 20$ °C) obtained by DLS and SLS shows a large difference. We believe that this difference arises from the ultra-soft nature of the particles, where the outermost loosely cross-linked shell swells considerably, mostly due to the presence of the internal confined counterions. This then results in a very low local polymer density in the shell and thus a very low scattering contrast. Effective volume fractions were determined from the relative viscosity measured with a capillary viscometer at low concentrations at $T = 20$ °C.[19]

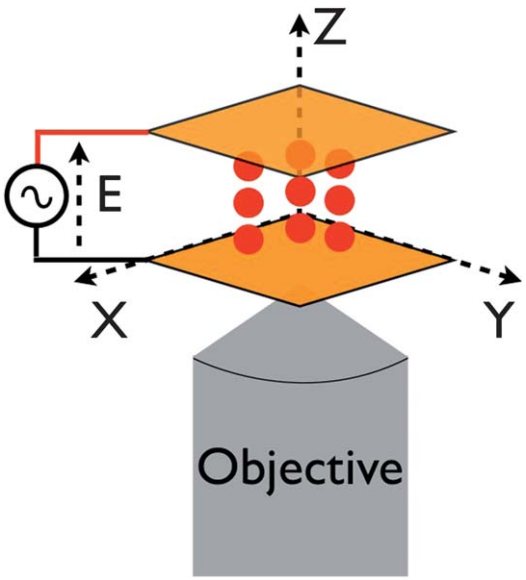

Fig. 1 Schematic picture of the field set-up. The suspension is kept between two ITO-coated cover glasses separated by a 120 μm spacer. An alternating electric field at a frequency of 100 kHz is applied along the *Z*-direction and observations are made in the *XY*-plane.

2.2 Confocal microscope and electric field geometry

All electric field studies were carried out using an inverted confocal laser scanning microscope (CLSM) (Leica DMI6000 with an SP5 tandem scanner in the resonant mode of 50 frames per s, an excitation wavelength of 543 nm and using a 63× or 100× immersion objective with a numerical aperture of 1.4). The fast resonant scanner allows us to accurately track particles even at low concentrations in the fluid state. The CLSM is mounted in a thermostatted enclosure, which enables temperature control with an accuracy of 0.2 degree. In the current study, we mostly worked at a constant temperature of 20 °C, and the number density was varied to perform experiments over a range of effective volume fractions from $0.07 \leq \phi_{\mathrm{eff}} \leq 0.66$. The samples were contained between two ITO-coated cover glasses separated by a spacer, resulting in a gap width of 120 μm, and measurements were made more than 10 particle diameters away from the cover slide to minimize wall effects. A schematic figure of the observation geometry is shown in Fig. 1. A sinusoidal electric field at a frequency of 100 kHz was applied along the *Z*-direction perpendicular to the image plane, and all the observations were made in the *XY*-image plane.

3 Results

An overview of the samples studied and a summary of our results are given in Fig. 2. At low ϕ_{eff}, we observe a field-induced fluid to string transition at intermediate field strength. At higher field strengths we observe an additional two phase

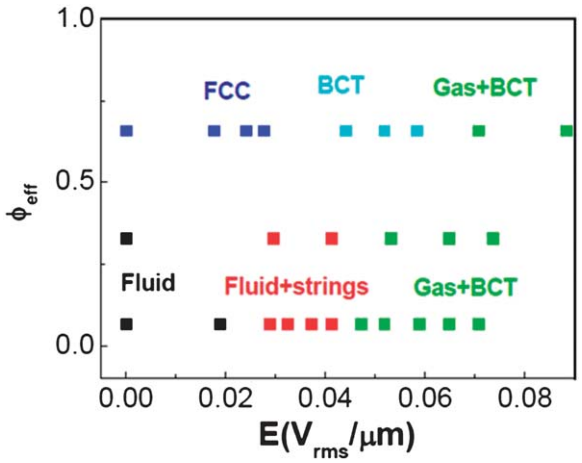

Fig. 2 Phase diagram of ionic microgels in the presence of a uniaxial alternating electric field at different ϕ_{eff} exhibiting, at lower packing fractions, transitions from fluid to fluid + string and gas + BCT coexistence, and at higher packing fractions, transitions from FCC to BCT to gas + BCT coexistence at a constant frequency of 100 kHz.

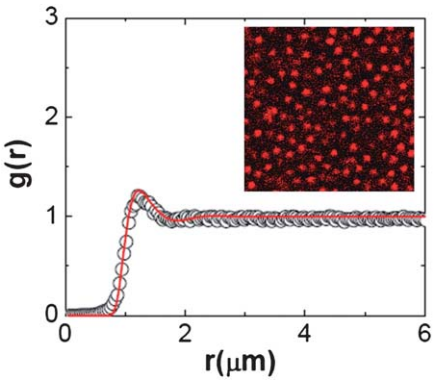

Fig. 3 Pair correlation function $g(r)$ for a microgel suspension at $\phi_{eff} = 0.07$, obtained in the fluid state using CLSM (typical image shown in the inset) together with a calculation based on a Yukawa potential.

region where a gas and a body centered tetragonal (BCT) phase coexist. This is consistent with our previous studies,[30] where we also found novel glass to crystal transitions at ultra-high effective packing fractions. In this work, we probe in detail the intermediate effective packing fraction, $\phi_{eff} = 0.66$, *i.e.* above the freezing line at zero field, where we observe a field-induced crystal (face centered cubic, FCC) to crystal (body centered tetragonal, BCT) transition. In the following, we discuss the different regions of the phase diagram and focus in particular on the FCC–BCT transition and the comparison to analogous field-induced transitions in hard-sphere like systems.

3.1 Zero-field phase behavior at low $\phi_{eff} = 0.07$

Ionic microgels possess a variable degree of softness and a tunable interaction potential that varies from a long-range Yukawa-like interaction at large separation distances to a much softer repulsive interaction (Hertzian type) at short distances.[27] At low ϕ_{eff} the ionic microgels thus mostly interact with a long-range Yukawa type interaction. This is demonstrated with a typical experimental pair correlation function $g(r)$ in the liquid state at low $\phi_{eff} = 0.07$ as obtained from CLSM using the methods described in our previous work[26] shown in Fig. 3. The number of effective charges per particle Z_{eff} was determined by fitting the experimental $g(r)$ to the theoretical prediction as calculated using liquid state theory based on the hyper netted chain HNC closure relationship with a Yukawa potential as described earlier.[30] From the fit, we obtained $Z_{eff} = 350e$ for the effective charge of the microgels, and a Debye screening length $\kappa^{-1} = 150$ nm.

3.2 Field driven phase behavior at low ϕ_{eff}

The field-induced behavior of the ionic microgels at different values of ϕ_{eff} and at different electric field strengths E (in V_{rms} μm^{-1}) with the field applied along the Z-direction (see Fig. 1) is illustrated with a series of two-dimensional (2D) CLSM images in Fig. 4. First we look at the field-driven phase behavior at $\phi_{eff} =$ 0.07 and 0.33 at a frequency of 100 kHz. At $E = 0$ the particles are initially in an isotropic liquid-like state with a homogeneous distribution in the field of view. At relatively low field values of $E = 0.041$ V_{rms} μm^{-1} at $\phi_{eff} = 0.07$, we observe an apparent decrease of the 2D number density in the field of view of the microscopy image plane with increasing E. From our previous study we know that under these conditions particle strings form along the field direction.[30] This was clearly demonstrated with a field applied along the X-direction instead, where the chains subsequently formed and aligned along the X-direction in the image plane. However, if the field is applied along the Z-direction, string formation takes place correspondingly along the Z-direction, and in the XY-plane we only see the 2D projection of a string that looks like a single particle in the image plane.

As the field strength is further increased, the chains start to associate laterally to form columnar aggregates, which appear in the XY-plane as clusters of 2–3 particles (*i.e.* strings) at $E =$ 0.041 V_{rms} μm^{-1} for $\phi_{eff} = 0.07$ and clusters of 4–5 particles (*i.e.* strings) for $\phi_{eff} = 0.33$. The driving force for this lateral attraction between individual strings is the sum of individual pairwise dipole–dipole interactions between spheres in two strings.[32] The result of this is that when two strings have a density modulation in Z that is in phase ("stacked"), the interaction is always repulsive, however, when they are out of phase by half an inter-particle spacing, then the interaction is attractive at short distances but repulsive at large distances. It is this attractive/repulsive interaction that, coupled with the soft repulsions, can give rise to a complex phase behavior.

At even higher field strengths, the aggregates increase in size and form well defined ordered lattice structures with a square symmetry in the XY-plane that is typical for BCT structures[3,4,30] as demonstrated in the snapshots shown in Fig. 4 at $E = 0.07$ V_{rms} μm^{-1} and 0.1 V_{rms} μm^{-1} for $\phi_{eff} = 0.07$ and for $E = 0.088$ V_{rms} μm^{-1} for $\phi_{eff} = 0.33$. It is interesting to point out that we find ring-like structures at $\phi_{eff} = 0.07$ and $E = 0.07$ V_{rms} μm^{-1}. A ring in the 2D projection is simply a sheet that closed in on itself. It has been shown that BCT structures are preferred to sheets above a threshold field and chain length.[3] However, it is possible that a small sheet that closes in on itself might have

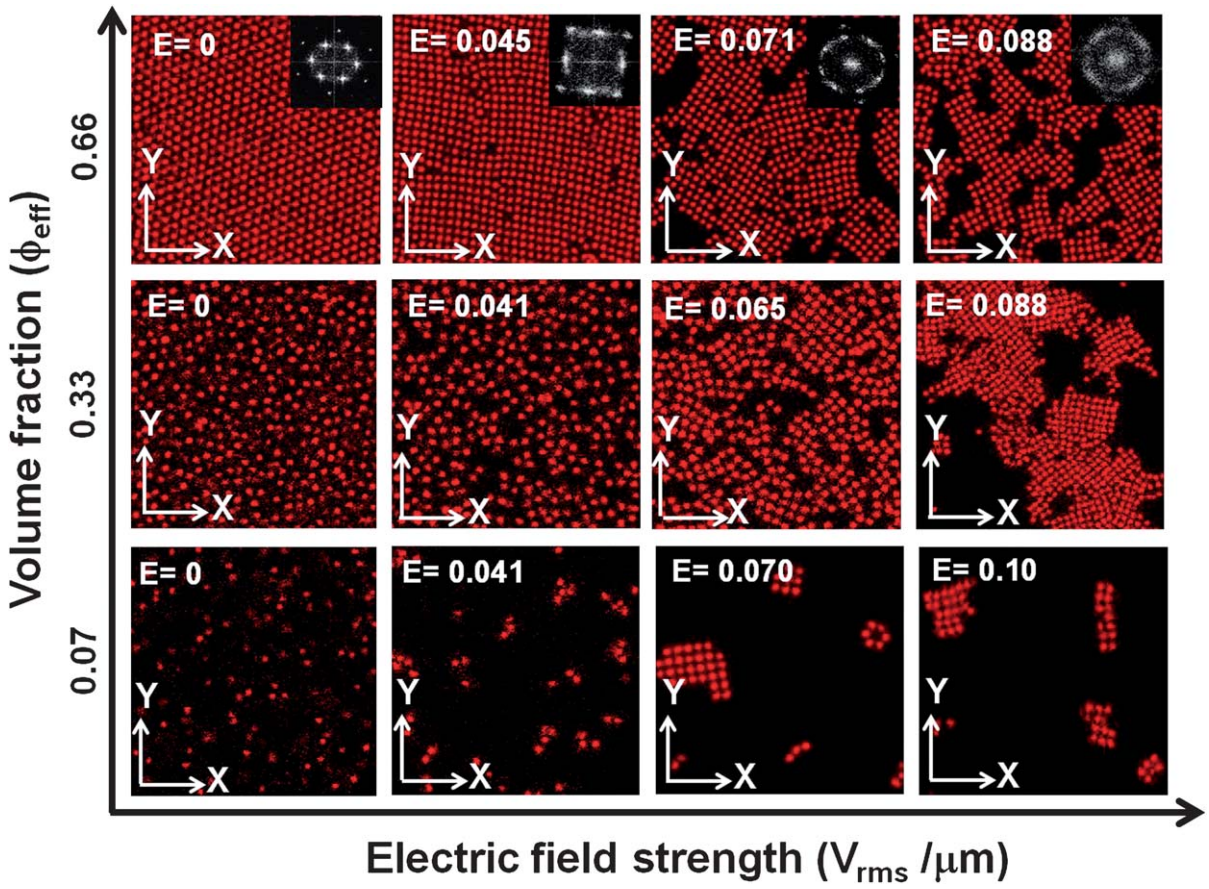

Fig. 4 2D confocal images taken in the bulk (10 particle diameters from the cover glass surface) with increasing field strength E (in V_{rms} μm^{-1}) at different ϕ_{eff} of 0.07, 0.33 and 0.66. The field direction is perpendicular to the image XY-plane. Also shown as insets are diffraction patterns obtained from a Fourier transform of the images at $\phi_{eff} = 0.66$.

comparable stability to a small BCT crystallite. These polycrystalline BCT structures coexist with a large space containing a few individual chains. The largest BCT crystallite observed had a size of around 7000 μm^3. The polycrystalline domain is comparatively larger for the higher $\phi_{eff} = 0.33$, as expected. The coexistence of BCT structures with an aggregate-free space (whose fraction changes with the overall packing fraction) is akin to that of a gas–solid transition as observed in the previous studies on hard sphere colloids under an external electric field[4,32] at low ϕ_{eff}. Hence our 2D phase diagram demonstrates a structural transition from an isotropic fluid to a string fluid and then to a coexistence of aggregates of string-gas and BCT states with increasing field strength for the two volume fractions of $\phi_{eff} = 0.07$ and 0.33.

It is also worth pointing out that recent experimental studies on highly polarized hard sphere magnetic colloids under zero-gravity conditions and with an external magnetic field have shown field induced chain-formation. It was further shown that chain aggregation leads to a percolated gel-like structure, which under annealing resulted in a BCT phase.[33] While the interparticle interactions in their work are different from those in the ultrasoft microgel colloids, their methods for annealing of the samples are likely transferable to our system.

The field-induced structural transitions are further quantified by calculating the pair-correlation functions $g(r)$ (Fig. 5A) and the corresponding mean square displacements $\langle \Delta r^2(t) \rangle$ (Fig. 5B) at $\phi_{eff} = 0.07$. At $E = 0$, the obtained data are consistent with a fluid-like structure and diffusive dynamics. We expect that with increasing E, particles will orient along the field direction Z to form strings, and hence the structural correlation will increase along the field direction and decrease in the XY-plane.[30] The corresponding particle dynamics in a chain perpendicular to the field direction is also expected to slow down as an additional manifestation of string formation. This behavior can indeed be seen in our calculated $g(r)$ and $\langle \Delta r^2(t) \rangle$ as a function of increasing E (Fig. 5A and B). With increasing E, we initially observe a decrease in the degree of spatial correlation as expressed by the peak height g_{max} of $g(r)$ (Fig. 5C), which starts to increase again around $E = 0.032$ V_{rms} μm^{-1}. The average interparticle separation a_s obtained from the position of the first peak appears to remain constant up to $E = 0.032$ V_{rms} μm^{-1} (Fig. 5D), and at the same time, $\langle \Delta r^2(t) \rangle$ (Fig. 5B) shows a decrease in the particle diffusivity at $E = 0.032$ V_{rms} μm^{-1} as clear indications of a fluid to string transition.

For $E > 0.032$ V_{rms} μm^{-1}, strings aggregate into clusters as shown in Fig. 5A at $E = 0.037$ and 0.041 V_{rms} μm^{-1}. This is confirmed by the increase in spatial correlation in $g(r)$, which shows as an increase of the peak height g_{max} (Fig. 5C). For $E >$ 0.041 V_{rms} μm^{-1}, the $g(r)$ now exhibits strong structural correlations indicative of a coexistence of a dilute string phase with a

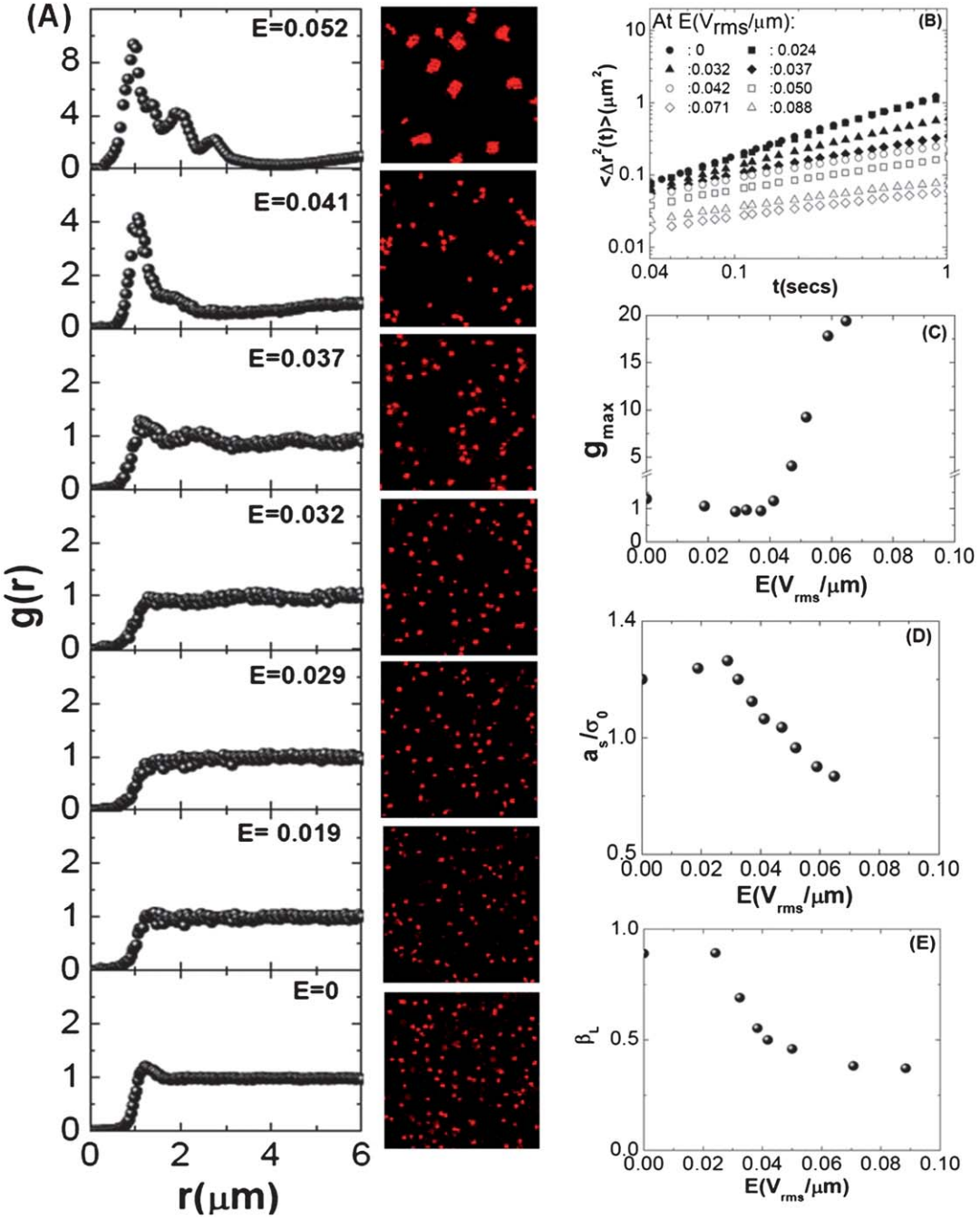

Fig. 5 (A) Pair-correlation function, $g(r)$ (left) and the corresponding 2D confocal image (right) at $\phi_{eff} = 0.07$ with increasing field strength E (in V_{rms} μm^{-1}). (B) Mean square displacement $\langle \Delta r^2(t) \rangle$ *vs.* time t (s) at different field strengths. (C) Peak height g_{max} of the first peak of $g(r)$ as a function of E. (D) Average interparticle separation a_s (calculated from the position of the first peak of the $g(r)$), normalized by the particle diameter σ_0 in the fully swollen state, *vs.* E. (E) The slope of the mean square displacement β_L as extracted from $\ln(\langle \Delta r^2(t) \rangle)$ *vs.* $\ln(t)$ as a function of E exhibits a decrease from a value close to 1 at zero electric field to a value less than 0.5 at high fields. g_{max} shows an upturn and a_s/σ_0 and β_L exhibit a sharp decrease above a threshold field ($E \sim 0.02$ to 0.04 V_{rms} μm^{-1}).

crystalline BCT phase. Moreover at $E > 0.032$ V_{rms} μm^{-1}, microgels in different strings start to overlap significantly due to their soft-repulsive nature, and hence we see a decrease of the average interparticle separation a_s lower than the diameter σ_0 of the microgel particle in the swollen state (Fig. 5D). At the same time, the particle dynamics slow down significantly and show signs of arrest as evidenced by the decrease of the slope of $\langle \Delta r^2(t) \rangle$ (Fig. 5B). The slope β_L extracted from $\ln(\langle \Delta r^2(t) \rangle)$ *vs.* $\ln(t)$ (Fig. 5E) reaches a plateau $E > 0.052$ V_{rms} μm^{-1}. Usually the local self-diffusion of particles perpendicular to E in a single chain will have several contributions, translational diffusions from the overall center of mass diffusion of the string, chain-fluctuations as well as local thermal fluctuations of the particles in their potential well.[34] Once individual strings assemble into larger aggregates, chain–chain interactions will additionally influence the local particle motions. This becomes evident at

higher field strengths, $E > 0.032\ V_{rms}\ \mu m^{-1}$. Due to the limited time resolution of CLSM, it is difficult to probe the short-time dynamics, and thus we cannot obtain information about the different processes. However, a more detailed study of the chain dynamics using dynamic light scattering is currently in progress, which allows us to probe particle dynamics over an extended range of times.

The field-dependent structural and dynamical quantities calculated at low values of ϕ_{eff} thus provide evidence of characteristic signatures of a fluid–string transition, chain-aggregation and finally a gas–BCT phase coexistence. Moreover, it is interesting to point out that the recent theoretical work of Brandt *et al.*,[15] where a dipolar fluid is modelled by a total effective pair-potential combining a repulsive Yukawa interaction with an added dipolar attraction, has predicted a structural signature of a fluid–string transition associated with the bifurcation of the angular averaged pair-correlation function $g_o(r)$. Their $g_o(r)$ shows a gradually decreased correlation with increasing dipolar strength when approaching the fluid–string transition. At the string–fluid transition, the bifurcation of the first peak results in two new correlation lengths characterizing the longitudinal and transverse order in string fluids. Although a gradual decrease is seen in our experimental 2D radial $g(r)$ perpendicular to the field direction, a one to one correspondence cannot be made, as our radial 2D $g(r)$ is not averaged over angles. However, this theoretical prediction can be verified through experiments by looking into the angle averaged correlation function along the field direction at a lower concentration where the chain–chain interactions can be avoided.

We can also compare our experimental results at low ϕ_{eff} to those of previous experimental and theoretical studies on hard sphere and charged colloids in the presence of an external electric field.[1,3,4,11,13] Previous theoretical studies[11] have predicted that the evolution of structure occurs in two stages. The particles first orient along the electric field to form chains, and then chains aggregate into dense structures that take the form of columns aligned along the electric field. These aggregates of chains (or columns) lead to a stable BCT state.[11] However, in previous experimental studies[3] using hard sphere colloids, two-dimensional sheet structures have been observed as an intermediate state before the formation of a stable BCT order. This is in contrast to our experimental observations where we find a stable BCT phase at a much lower field strength compared to the previous studies,[3,4] and without experimental evidence for an intermediate sheet formation.

3.3 Field-induced phase behavior at $\phi_{eff} = 0.66$

We next look into the field-dependent phase behavior of the microgel suspension at $\phi_{eff} = 0.66$. At zero field, the sample crystallizes. A raw 2D image of the crystalline order is shown in Fig. 6A at $T = 20\ ^\circ C$. This zero-field crystalline state shows all the characteristic features of a face-centered cubic (FCC) structure

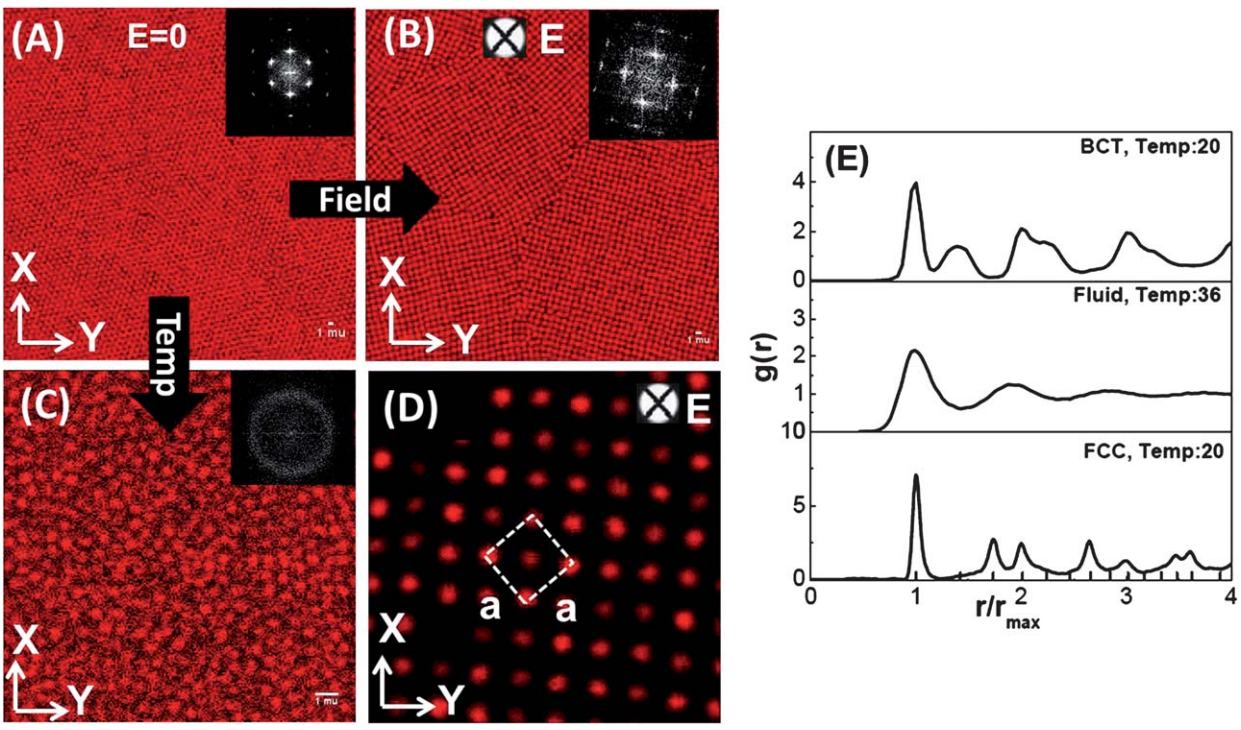

Fig. 6 Electric field and temperature driven phase transitions at an intermediate packing fraction $\phi_{eff} = 0.66$: an increasing electric field drives a crystal-to-crystal transition, while an increasing temperature drives a crystal-to-fluid transition. This is demonstrated with 2D confocal images taken in bulk suspensions at constant number density. Also shown as insets are diffraction patterns obtained from a Fourier transform of the images. (A) Zero-field FCC crystalline order at $\phi_{eff} = 0.66$ at a temperature of $T = 20\ ^\circ C$. (B) Field-induced BCT state at $E = 0.045\ V_{rms}\ \mu m^{-1}$ and $T = 20\ ^\circ C$. (C) Fluid state obtained by melting the zero-field FCC crystal phase at a temperature of $T = 36\ ^\circ C$. (D) Magnified image together with the square lattice. (E) The corresponding pair-correlation functions $g(r)$ for each state shown in (A)–(C).

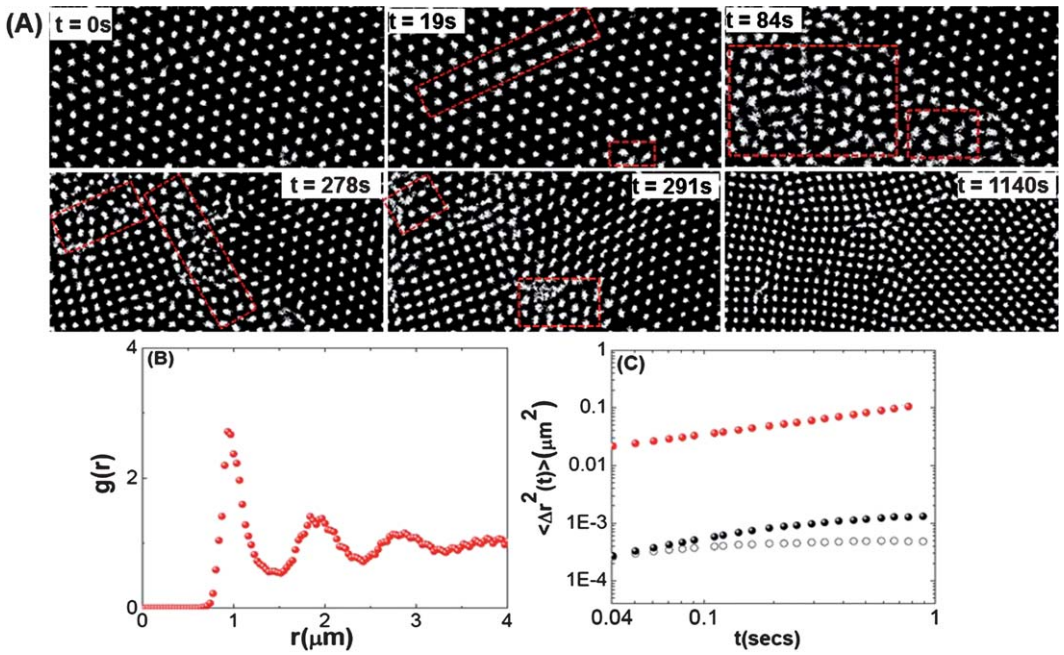

Fig. 7 (A) Time evolution of the 2D particle trajectories in the *XY*-plane over 300 frames (=6 s) at $\phi_{eff} = 0.66$ after the application of an electric field at $E = 0.045$ V_{rms} μm^{-1}. Also shown is the corresponding structure with the pair correlation function $g(r)$ (B) and the dynamics represented by the mean square displacement $\langle \Delta r^2(t) \rangle$ (C) calculated in the disordered region at $t = 84$ s, respectively. In (C), the mean square displacement, $\langle \Delta r^2(t) \rangle$ (red circles) calculated in the disordered region, is compared with that of $\langle \Delta r^2(t) \rangle$ from a FCC (black open circles) and BCT crystalline state (black filled circles), respectively.

when looking at the peak positions of the experimentally determined $g(r)$ (Fig. 6E).

By subjecting this FCC crystal to an electric-field $E = 0.045$ V_{rms} μm^{-1}, we find a field-induced crystal (FCC)–crystal (dipolar BCT) transition, as shown in Fig. 6B, and a gas–BCT coexistence at a higher $E = 0.071$ and 0.088 V_{rms} μm^{-1}, as shown in Fig. 4 (top panel). The field-induced dipolar ordered state is a polycrystalline domain with a square symmetry. As can be seen from the magnified image (Fig. 6D) perpendicular to the field direction, the BCT structure can be constructed by placing strings of particles into two interpenetrating square lattices ($a = b$), where the particles in the strings are displaced by $c/2$ along the *Z*-direction. The unit cell spacing in the *XY*-plane is extracted from the measured first peak position of the calculated 2D $g(r)$ (Fig. 6E) where $a = b = \sqrt{3/2} \sim 1.22$ μm. The corresponding unit cell spacing along the *Z*-direction is calculated to be $c = 2a/\sqrt{6} \sim 0.996$ μm.

Due to the thermo-responsive nature of the microgel particle, this crystalline state can also be melted into a fluid state at a temperature above the LCST, which is demonstrated in Fig. 6C with the corresponding fluid $g(r)$ (Fig. 6E) at $T = 36$ °C. This dual control – a field driven crystal-to-crystal transition and a temperature driven crystal-to-fluid transition – not only allows us to anneal crystal structures through temperature-induced melting and freezing steps, but opens the door to kinetic studies of the melting and freezing transitions. Below we report preliminary results that are indicative of the opportunities provided by this intermediate region in the E–ϕ_{eff} phase diagram.

At $\phi_{eff} = 0.66$, we follow the transient kinetics of the FCC to BCT transition by following particle trajectories (in 2D) after the field is turned on (Fig. 7A). After 19 s we see that the zero-field crystalline state with hexagonal symmetry starts melting into a small patch of a disordered region. After 84 s, this small disordered region starts to grow slowly. The disordered region is highlighted by a rectangular dashed box in the different images of Fig. 7. After 291 s, this disordered region structurally rearranges into a region with square symmetry, which coexists with the zero-field crystalline state and a small patch of disordered particles. The snapshot at 1140 s shows that the structure now is mostly of square-like symmetry.

The intermediate melting and subsequent re-crystallization is also demonstrated by quantitative analysis of the structure and dynamics at an intermediate time $t = 84$ s. The $g(r)$ from the disordered region is shown in Fig. 7B. A comparison of the $\langle \Delta r^2(t) \rangle$ calculated in the disordered region (red circles) with that of the $\langle \Delta r^2(t) \rangle$ in the FCC (black open symbols) and BCT (black closed symbols) crystalline state confirms that the disordered region is in a liquid state with a higher diffusivity.

These qualitative observations are further supported by calculating the distribution of the 2D local bond-order parameters[35] ψ_6 and ψ_4 through a Voronoi map for both zero-field crystalline order at $t = 0$ s (Fig. 8A), and at times $t = 84$ and $t = 1140$ seconds (Fig. 8B and C). In the Voronoi map, regions with $\psi_6 > 0.7$ are colored red and denote high six-fold symmetry, while regions with $\psi_4 > 0.7$ are blue and denote high four-fold symmetry, and white regions denote particles with both ψ_6 and ψ_4 below 0.7. For the zero-field crystalline order at $t = 0$, the global $|\psi_6| = 0.83$, with approximately 83% of the particles exhibiting strong 6-fold symmetry coexisting with 16% of regions that are disordered. Disordered regions can arise due to

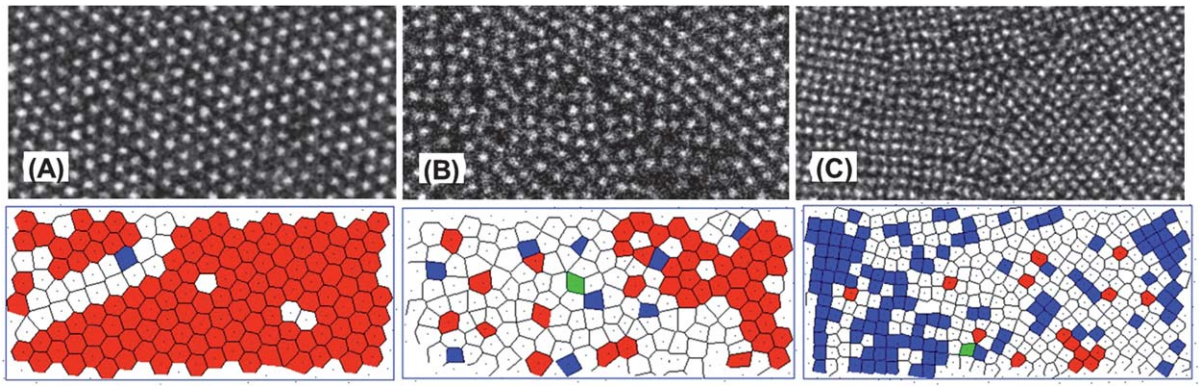

Fig. 8 Graphical representations of a bond order correlation analysis of the temporal evolution of the structure at $\phi_{eff} = 0.66$ after the application of an electric field at $E = 0.045\ V_{rms}\ \mu m^{-1}$. Top row: snapshots of CLSM images at $t = 0$ s (A), 84 s (B) and 1140 s (C), respectively. Bottom row: Voronoi map with color coding for bond order analysis. Color code: red: $\psi_6 > 0.7$; blue: $\psi_4 > 0.7$; white: $\psi_6 < 0.7$ and $\psi_4 < 0.7$; green: $\psi_6 > 0.7$ and $\psi_4 > 0.7$ (rarely or never happens).

defects, dislocations, lattice distortions or grain boundaries. The Voronoi map at $t = 84$ seconds is dominated by relatively disordered regions (about 66% of the particles). Finally, the snapshot at $t = 1140$ seconds (Fig. 8C, with global $|\psi_4| = 0.63$) shows that around 33% of the particles have already transformed into regions of high 4-fold symmetry and coexist with regions of low ψ_4 that are primarily disordered. These preliminary results confirm that the field-driven crystal to crystal transition observed here indeed occurs *via* a melting or structural disordering process. While this is apparently very different from previously studied dipolar hard sphere[5] and charged colloidal systems,[36] we must be cautious in our conclusions because the extent of this transient restructuring is likely to be sensitively dependent on the direction of the field with respect to the FCC crystal *c* axis. Taking into account the non-uniformities of the internal electric field due to the presence of the particles themselves, the electric field intensity is higher at the interstitial sites between particles in a chain.[37,38] This is believed to lead to a strengthening of the propensity for close-packed structures, and might affect the FCC-to-BCT transition quantitatively.

Crystal to crystal transitions known as martensitic transformations[39] are well known in atomic systems. Here the atoms move cooperatively relative to their neighbors, and this cooperative movement gives rise to a new crystal structure. Colloidal analogues of this diffusionless martensitic transition have also been found under the influence of an external electric field for hard sphere and charged colloids,[3–5] or in a confined geometry[36] using charged colloids. In these studies, no intermediate melting process has been observed. We can currently only speculate that the different behavior of our ionic microgels documented in Fig. 7 is due to the ultra-soft nature of the interaction potential between the ionic microgels and its intricate interplay with the added dipolar interactions. Even at zero-field, the density-driven theoretical phase diagram of ionic microgels[28] has shown different types of stable crystalline states accompanied by a re-entrant melting, and this melting phenomenon does not obey conventional melting criteria as seen in the case of charged or hard sphere colloids. A detailed kinetic study of this field-induced transformation for different degrees of softness is thus clearly required.

4 Conclusions

Ionic microgels with their ultrasoft interaction potential and a large amount of confined counterions are very attractive model systems for the investigation of field-directed self-assembly. Not only do they allow for a completely tuneable strong anisotropic contribution to the interaction potential, but their thermoresponsive nature provides an additional externally controllable parameter to reversibly induce phase transitions and anneal the final structure and dynamics. Our results also indicate that the ultrasoft potential and the ability of the particles to interpenetrate and deform lead to distinctly different phase transition scenarios when compared to the previously studied hard colloids. It is however clear that additional and detailed investigations of these systems at different degrees of softness are needed.

Acknowledgements

This work was supported by the Swiss National Science Foundation, the Swedish Research Council (Project 621-2011-4338), the Faculty of Science of Lund University and the Natural Sciences and Engineering Research Council of Canada (NSERC). PS and PSM acknowledge Dr Martin Medebach for illuminating discussions.

References

1 R. Tao and J. Sun, *Phys. Rev. Lett.*, 1990, **65**, 2820.
2 J. Martin, J. Odinek, T. Halsey and R. Kamien, *Phys. Rev. E: Stat. Phys., Plasmas, Fluids, Relat. Interdiscip. Top.*, 1998, **57**, 756.
3 U. Dassanayake, S. Fraden and A. van Blaaderen, *J. Chem. Phys.*, 2000, **112**, 3851.
4 A. Yethiraj and A. van Blaaderen, *Nature*, 2003, **421**, 513.

5 A. Yethiraj, A. Wouterse, B. Groh and A. van Blaaderen, *Phys. Rev. Lett.*, 2004, **92**, 058301.
6 M. E. Leunissen, H. R. Vutukuri and A. van Blaaderen, *Adv. Mater.*, 2009, **21**, 2116.
7 J. M. McMullan and N. J. Wagner, *Soft Matter*, 2010, **6**, 5443.
8 W. M. Winslow, *J. Appl. Phys.*, 1949, **20**, 1137.
9 M. Parthasarathy and D. Klingenberg, *Mater. Sci. Eng., R*, 1996, **17**, 57.
10 S. Fraden, A. J. Hurd and R. Meyer, *Phys. Rev. Lett.*, 1989, **63**, 2320.
11 T. Halsey and W. Toor, *Phys. Rev. Lett.*, 1990, **65**, 2820.
12 K. Zhang and X. Liu, *Phys. Rev. Lett.*, 2004, **92**, 058301.
13 A. Hynninen and M. Dijkstra, *Phys. Rev. E: Stat., Nonlinear, Soft Matter Phys.*, 2005, **72**, 051402.
14 A. Yethiraj, *Soft Matter*, 2007, **3**, 1099–1115.
15 P. C. Brandt, A. V. Ivlev and G. E. Morfill, *J. Chem. Phys.*, 2010, **132**, 234709.
16 C. N. Likos, H. Löwen, M. Watzlawek, B. Abbas, O. Jucknischke, J. Allgaier and D. Richter, *Phys. Rev. Lett.*, 1998, **80**, 4450.
17 D. M. Heyes and A. C. Branka, *Soft Matter*, 2009, **5**, 2681.
18 L. Berthier, A. J. Moreno and G. Szamel, *Phys. Rev. E: Stat., Nonlinear, Soft Matter Phys.*, 2010, **82**, 060501R.
19 H. Senff and W. Richtering, *J. Chem. Phys.*, 1999, **111**, 1705.
20 M. Stieger, W. Richtering, J. S. Pedersen and P. Lindner, *J. Chem. Phys.*, 2004, **120**, 6197.
21 M. Das, H. Zhang and E. Kumacheva, *Annu. Rev. Mater. Res.*, 2006, **36**, 117.
22 D. A. Sessoms, I. Bischofberger, L. Cipelletti and V. Trappe, *Philos. Trans. R. Soc., A*, 2009, **367**, 5013.
23 Z. Meng, V. B. Jae Kyu Cho and L. A. Lyon, *J. Phys. Chem. B*, 2009, **113**, 4590.
24 F. Scheffold, P. Diaz-Leyva, M. Reufer, N. B. Braham, I. Lynch and J. L. Harden, *Phys. Rev. Lett.*, 2010, **104**, 128304.
25 Z. Zhang, N. Xu, D. T. N. Chen, P. Yunker, A. M. Alsayed, K. B. Aptowicz, P. Habdas, A. J. Liu, S. R. Nagel and A. G. Yodh, *Nature*, 2009, **459**, 230.
26 D. Paloli, P. S. Mohanty, J. J. Crassous, E. Zaccarelli and P. Schurtenberger, *Soft Matter*, 2013, **9**, 3000.
27 J. Riest, P. Mohanty, P. Schurtenberger and C. N. Likos, *Z. Phys. Chem.*, 2012, **226**, 711.
28 D. Gottwald, C. Likos, G. Kahl and H. Löwen, *Phys. Rev. Lett.*, 2004, **92**, 068301.
29 P. S. Mohanty and W. Richtering, *J. Phys. Chem. B*, 2008, **112**, 14692.
30 P. S. Mohanty, A. Yethiraj and P. Schurtenberger, *Soft Matter*, 2012, **8**, 10819.
31 M. Mittal, P. P. Lele, E. W. Kaler and E. M. Furst, *J. Chem. Phys.*, 2008, **129**, 064513.
32 A. M. Almudallal and I. Saika-Voivod, *Phys. Rev. E: Stat., Nonlinear, Soft Matter Phys.*, 2011, **84**(5), 011402.
33 J. W. Swan, P. A. Vasquez, P. A. Whitson, E. M. Fincke, K. Wakata, S. H. Magnus, F. D. Winne, M. R. Barratt, J. H. Agui, R. D. Green, N. R. Hall, D. Y. Bohman, C. T. Bunnell, A. P. Gast and E. M. Furst, *Proc. Natl. Acad. Sci. U. S. A.*, 2012, **109**, 16023.
34 M. Hagenbüchle and J. Liu, *Appl. Opt.*, 1997, **36**, 7664.
35 M. J. McDonald, A. Yethiraj and L. Y. Beaulieu, *Meas. Sci. Technol.*, 2012, **23**, 045606.
36 J. A. Weiss, D. W. Oxtoby, D. G. Grier and C. A. Murray, *J. Chem. Phys.*, 1995, **103**, 1180.
37 F. Smallenburg, H. Vutukuri, A. Imhof, A. van Blaaderen and M. Dijkstra, *J. Phys.: Condens. Matter*, 2012, **24**, 464113.
38 B. Bharti, G. H. Findenegg and O. D. Velev, *Sci. Rep.*, 2012, **2**, 1004.
39 W. C. Kerr, M. G. Killough, A. Saxena, P. J. Swart and A. R. Bishop, *Phase Transitions*, 1999, **69**, 270.